Geophysical Research Letters

RESEARCH LETTER
10.1029/2023GL103417

Impacts of Mesoscale Cloud Organization on Aerosol-Induced Cloud Water Adjustment and Cloud Brightness

Xiaoli Zhou[1,2] **and Graham Feingold**[1]

[1]Chemical Sciences Laboratory, NOAA, Boulder, CO, USA, [2]Cooperative Institute for Research in Environmental Sciences (CIRES), University of Colorado, Boulder, CO, USA

Key Points:

- Mesoscale cellular convection (MCC) cell-size significantly regulates aerosol-induced cloud albedo via its effect on cloud water adjustment
- The aerosol-induced cloud water adjustment in small-scale MCCs can be 10 times more negative than in large-scale MCCs
- We find notable intra-cell co-variability between cloud liquid water path and drop concentration within MCCs that varies with cell size

Supporting Information:

Supporting Information may be found in the online version of this article.

Correspondence to:

X. Zhou,
xiaoli.zhou@noaa.gov

Citation:

Zhou, X., & Feingold, G. (2023). Impacts of mesoscale cloud organization on aerosol-induced cloud water adjustment and cloud brightness. *Geophysical Research Letters*, *50*, e2023GL103417. https://doi.org/10.1029/2023GL103417

Received 22 FEB 2023
Accepted 1 JUN 2023

Abstract The role of mesoscale cellular convection (MCC) in regulating aerosol-induced cloud brightness remains unaddressed. Using 7 years of satellite-based observations of cloud water adjustment to aerosol-induced perturbations for closed MCCs across different sizes (8, 16, 32, and 64 km) over the North Atlantic Ocean, we show that MCC cell-size plays a nontrivial role in regulating aerosol-induced cloud brightness via cloud water adjustment. In cells that are primarily non-precipitating, the adjustment in small-scale MCCs can be 10 times more negative than in large-scale MCCs, consistent with stronger evaporation via cloud top entrainment. Consequently, the response of cloud brightness is significantly stronger for large-scale MCCs. We also find notable intra-cell co-variability between cloud liquid water path (LWP) and drop concentration (N_d) within MCCs that varies with cell size. Erroneously considering such co-variability as a LWP response to N_d can lead to a significant positive bias, especially for small scale MCCs.

Plain Language Summary Low clouds over the ocean often exhibit organized patterns with characteristic cell sizes but the effect of this organization on cloud-aerosol interactions is not yet fully understood. Here we group 7 years of satellite-measured low cloud cells over the North Atlantic Ocean by their cell size to investigate how cell size influences the response of cloud water and cloud brightness to cloud droplet number concentration perturbations. Large-scale cells are found to have less efficient depletion of cloud water in response to increasing drop number compared to small-scale cells. This leads to nearly an order of magnitude stronger increase in cloud brightness with increasing drop number. Furthermore, we show that the spatial distributions of liquid water path and drop concentration vary with cell-size. Mistakenly assuming the local correlation between cloud water path and drop concentration to be a causal response can cause a significant positive error, especially for small-scale cells.

1. Introduction

Mesoscale organization of marine stratocumulus with cell sizes between ~10 and ~100 km, manifesting as mesoscale cellular convection (MCC, Agee et al., 1973), is ubiquitous and important in modulating cloud water, precipitation (e.g., Terai et al., 2014; Wood & Bretherton, 2006), and cloud albedo (Cahalan et al., 1994; McCoy et al., 2017; Stephens, 1986). Efforts have been made to improve understanding of MCCs and their radiative impact in the current climate, including quantification of cloud water inhomogeneity and cloud fraction (Wood & Bretherton, 2006; Wood & Taylor, 2001), climatology of MCC morphology (Lang et al., 2022; Yuan et al., 2020), evaluation of the thermodynamic environments of closed and open MCCs (Eastman et al., 2021; Jensen et al., 2021; McCoy et al., 2017; Terai et al., 2014) at various cell sizes (Zhou, Bretherton, et al., 2021; Zhou, Zhang, & Feingold, 2021), elucidation of the mechanism of mesoscale cellular circulations (Zhou & Bretherton, 2019b; Zhou et al., 2017, 2018), and understanding the impact of cloud phase on organizational patterns (Danker et al., 2021; Geerts et al., 2022; Tornow et al., 2021).

In terms of future climate, MCC morphology has been shown to have a nontrivial contribution (~0.07 W m^{-2} K^{-1}) to the shortwave cloud feedback, based on the environmental dependence of MCC morphology in the current climate (McCoy et al., 2022). This contribution may vary as aerosol indirect forcing changes in a future warmer world, yet the effect of anthropogenic atmospheric aerosol on MCC morphology remains poorly understood.

Anthropogenic aerosol is known to impact cloud radiative forcing through changes in cloud amount and brightness (e.g., Albrecht, 1989). Recent studies have quantified the cloud water adjustment and cloud albedo susceptibility to aerosol perturbations via ship tracks and satellite observations (e.g., Chen et al., 2014; Gryspeerdt et al., 2019; Possner et al., 2020; Zhang et al., 2022; Zhou, Bretherton, et al., 2021; Zhou, Zhang, & Feingold, 2021). These

studies, however, were conducted in the context of single layer warm clouds without considering the MCC properties. Here, we take a first look at the response of MCC cloud water to aerosol-induced drop concentration perturbations at different cell sizes, with a focus on closed cell MCCs.

A common way to quantify cloud water adjustment to aerosol perturbations via satellite observations is through computing the slope of the linear regression between retrieved liquid water path (LWP) and cloud droplet number concentration (N_d) within satellite snapshots of 1°–2° spatial scale. A potential issue with this approach, especially using high resolution retrievals, is that the computed slope might reflect the correlation between LWP and N_d at the mesoscale, rather than the response of cloud water to N_d. It is therefore critical to understand whether there is any correlation between LWP and N_d within a mesoscale cell.

The objective of this paper is twofold. (a) to quantify aerosol-induced perturbations of LWP for closed-cell MCCs of different cell size and (b) to investigate the intra-cell correlations between LWP, N_d, and effective radius of cloud droplets (r_e), for MCC closed cells and their relationships to cell size. We show that the LWP adjustment is negative overall, much more so for small scale MCCs than for large scale ones, especially for non-precipitation dominant cells where the LWP adjustment in small scale MCCs can be as much as tenfold more negative than in large scale cells. This result may have important implications for aerosol indirect forcing and future climate projection. We also find notable intra-cell co-variability between LWP and N_d at mesoscale within MCCs, which varies with cell size. Erroneously considering such co-variability as a LWP response to N_d can lead to a significant positive bias in cloud albedo susceptibility, especially for small scale MCCs.

2. Data and Methodology

We use 7 years (2005–2011) of the National Aeronautics and Space Administration (NASA) A-Train satellite measurements and European Center for Medium range Weather Forecast (ECMWF)'s fifth generation atmospheric reanalysis (ERA5) over the North Atlantic Ocean (25°–55°N; 50°–15°W) pertaining to single-layer liquid phase clouds.

Cloud properties including LWP, r_e, and cloud optical depth (τ) are sourced from Collection 6.1 daytime (~13:30 p.m. local time) marine cloud retrievals at 1 km (nadir) resolution from the MODerate-resolution Imaging Spectroradiometer (MODIS) on the Aqua satellite (Platnick et al., 2003, 2015). While r_e and τ are near-independent retrievals (Nakajima & King, 1990), LWP is based on the product of r_e and τ. N_d is derived from MODIS-retrieved τ and r_e following Grosvenor et al., 2018. We assume clouds are close to adiabatic with $f_{ad} = 0.8$, as supported by previous studies (Albrecht et al., 1990; Wood & Taylor, 2001). Clouds with $\tau < 3$ are considered too thin for a reliable N_d retrieval and are removed from the analysis. Cloud albedo is sourced from the Clouds and Earth's Radiant Energy System (CERES; Minnis et al., 2020) at a footprint resolution of 0.2° following $A_c = (A_{all} - A_{clr}(1 - f_c))/f_c$, where A_{all} is the all-sky albedo, computed as the ratio of upward to incoming solar irradiance at the top-of-atmosphere (TOA) measured by CERES, A_{clr} is the clear sky albedo sourced from ERA5, and f_c is the low-level cloud fraction within the CERES footprint. All CERES and ERA5 variables are re-grided onto the CERES resolution (0.2°) using nearest-neighbor interpolation before calculating A_c. To ensure robust estimation, here A_c is calculated for clouds with pixel-level cloud fraction greater than 20%.

To classify closed cellular MCCs by their dominant cell scales, we divide the domain into 2° × 2° latitude-longitude scenes. Following Zhou, Bretherton, et al. (2021) (Z21), we apply a two-dimensional (2D) wavelet analysis (Daubechies & Bates, 1993; Mallat, 1989a, 1989b; Meyer, 1992) to MODIS-retrieved LWP to identify a dominant MCC scale. Here we adopt Daubechies' orthogonal wavelet (Daubechies, 1988) as our analyzing mother wavelet, with filter length set to 5. In each 2° × 2° scene, we apply 2D forward and inverse discrete wavelet transforms as a band-pass filter bank in space to partition a spatial field of LWP into local fluctuations at four scale octaves ($8(2)^{-1/2} - 8 \times 2^{1/2}$ km, $16(2)^{-1/2} - 16 \times 2^{1/2}$ km, $32(2)^{-1/2} - 32 \times 2^{1/2}$ km, $64(2)^{-1/2} - 64 \times 2^{1/2}$ km) into which the majority of MCC scenes over the North Atlantic Ocean fall. These octaves are referred to by the weighted averages of their wavelength ranges, namely 8, 16, 32, and 64 km (see Z21 for a mathematical derivation). The cell scale is identified as the wavelength of the peak variance of the local LWP fluctuations. We restrict our analysis to MCC scenes with scene-level cloud fraction greater than 0.8. The high cloud fraction ensures that the characteristic cell scale is dominated by closed cellular MCC, rather than the biased scale caused by mesoscale patches of clear sky embedded in a closed cell region.

We apply the results of 2D wavelet cell size classification to N_d and r_e fields for each MCC scene, and compute the correlation between local fluctuations in LWP and N_d, and in LWP and r_e, filtered to the cell scale (by zeroing out

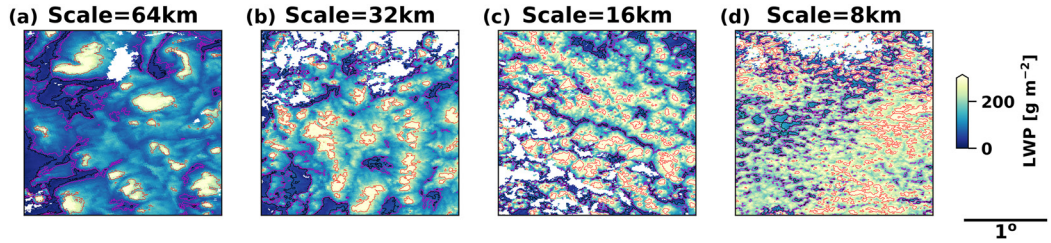

Figure 1. Example scenes (2° × 2°) of MODerate-resolution Imaging Spectroradiometer liquid water path (LWP) for MCCs of (a) 64 km, (b) 32 km, (c) 16 km, and (d) 8 km. The red, magenta, and black lines represent the contours of the top 10%, bottom 10%, and bottom 20% of LWP in each scene. A 1° length scale is depicted on the figure.

all of the coefficients of the wavelet-transformed matrix except for those at the cell scale wavelength). Hereafter we refer to this correlation as intra-cell correlation. We note that intra-cell correlation constitutes the majority of the total correlation while eliminating correlations caused by other non-dominant scales (Figure S1 in Supporting Information S1).

3. Intra-Cell Correlations Between LWP, N_d, and r_e

Figure 1 shows the example scenes of MODIS LWP at cells sizes from 8 to 64 km classified by the wavelet method. Cellular structures at various scales show up quite distinctly. In total, there are 2,461 scenes of 64 km cells, 2,298 of 32 km cells, 1,238 of 16 km cells, and 286 of 8 km cells.

In an attempt to understand the correlations between LWP, N_d, and r_e within cells, we compute the intra-cell correlation (defined in Section 2) between LWP and r_e, and between LWP and N_d for cells of different sizes as shown in Figures 2a and 2b. Intra-cell correlation between LWP and r_e increases noticeably with cell size, with the median value ranging from ∼0.35 at 8 km scale to ∼0.6 at 64 km (Figure 2a). Similar dependence on cell size is seen for the intra-cell correlation between the near-independent retrievals of τ and r_e (Figure S2 in Supporting Information S1). This provides confidence that Figure 2a represents a physical manifestation of the correlation of LWP with r_e rather than being a result of how LWP is derived (i.e., ∝ the product of r_e and τ). Since the N_d retrieval is strongly inversely related to r_e, intra-cell correlation between LWP and N_d decreases significantly with increasing cell size, with the median value ranging from ∼0.4 at 8 km to ∼0.03 at 64 km scale. Nearly

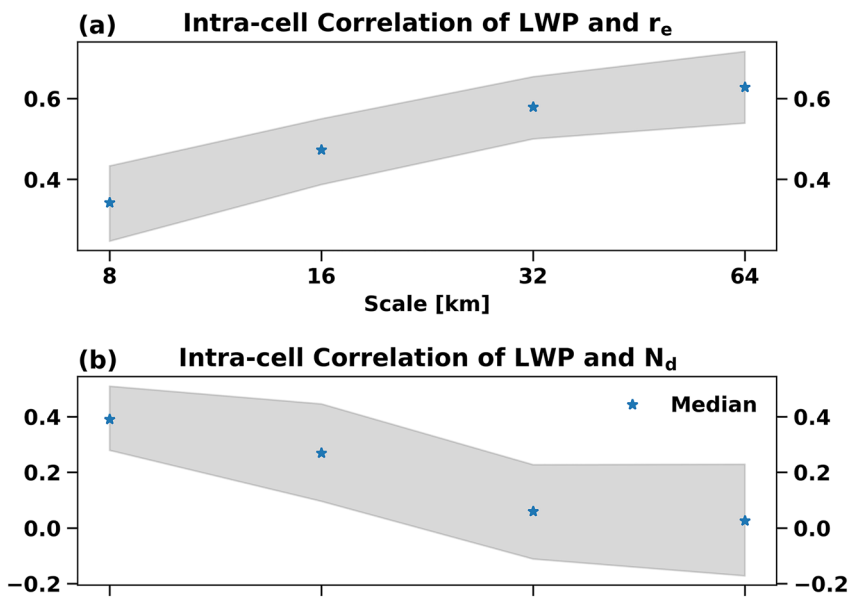

Figure 2. Intra-cell correlations between (a) liquid water path (LWP) and r_e, and (b) LWP and N_d for MCCs of 8, 16, 32, and 64 km. Stars indicate median values. Shading indicates the interquartile range.

half of the 64 km cells show negative correlations (Figure 2b). This progressive decrease with cell size is also reflected in total correlation (Figure S1 in Supporting Information S1). This result suggests that for MCCs with relatively large sizes, thicker cell centers contain cloud droplets much larger in size than those at the peripheries of the cell. For MCCs with relatively small sizes, thicker cell centers usually contain more numerous cloud droplets compared to cloud peripheries, whereas for large-size MCCs, N_d in thicker cell centers is comparable to, and sometimes even smaller than that at cloud peripheries. An illustration can be seen in Figures S3 and S4 of Supporting Information S1 which show scenes of N_d and r_e for the MODIS example scenes in Figure 1. Figure S5 in Supporting Information S1 quantifies the median N_d in each LWP bin for the example scenes.

We proffer two reasons for the difference in intra-cell correlation between LWP and N_d across cell sizes. One explanation might be related to the dynamical difference in cells of different size. Large scale MCCs are found to be more decoupled and less efficient in supplying moisture and total kinetic energy than small scale MCCs (Kazil et al., 2017). This will have consequences for both LWP and N_d sources and sinks, with concomitant effects on the intra-cell correlation between LWP and N_d. For example, in large scale MCCs, the stronger decoupled state impedes the transportation of aerosol into the clouds, causing the N_d source through activation in cell centers to be outweighed by the N_d depletion by precipitation scavenging, resulting in a stronger negative LWP-N_d correlation with increasing scale (Figure 2b). Another explanation might lie in the LWP distribution difference in cells of different size. Cells of relatively large size tend to have a more positively skewed LWP distribution implying a greater portion of thin cloud peripheries, yet much thicker cloud centers (Figure S6 in Supporting Information S1). Since drizzle formation is a strongly increasing function of LWP (e.g., Nicholls, 1987), MCCs of relatively large size might have a clearer separation of precipitating centers and non-precipitating peripheries, such that cloud droplets are actively scavenged in cloud centers but not in peripheries, favoring a weak positive to negative intra-cell correlation between LWP and N_d. In contrast, for MCCs of small cell size, LWP is more normally distributed, with more homogeneous drizzle (if any), which favors homogeneous depletion of N_d.

The distinct cell-size-dependent intra-cell co-variability between LWP, N_d, and r_e is a cautionary note to the approach of using the slope of linear regression within satellite snapshots as a proxy for LWP response to N_d (See further discussion in Section 5).

4. Responses of LWP to N_d Across Cell Sizes

To bypass the aforementioned mesoscale intra-cell co-variability bias, it is important that the mesoscale cell be considered as a non-segregated system that redistributes cloud water and droplets via mesoscale circulation even though aerosol activation occurs at small scales. As a result, aggregation is needed over a domain that can cover the entire cell. Here we quantify LWP adjustment to aerosol-induced perturbations by examining $2° \times 2°$ scene-average LWP of the cloudy MODIS pixels ($\overline{\mathrm{LWP}}$), and considering scene-average N_d of the cloudy MODIS pixels ($\overline{N_d}$) as a proxy for the surrounding aerosol in each scene.

The dependence of $\overline{\mathrm{LWP}}$ on $\overline{N_d}$ across cell sizes is reflected in Figure 3a which shows median values and interquartile ranges (IQRs) of $\overline{\mathrm{LWP}}$ in each percentile bin of $\overline{N_d}$ for scenes of different MCC cell sizes. The results are presented on logarithmic scales and hence the slope of distribution (as quantified by $L_0 = \mathrm{dln}(\overline{\mathrm{LWP}})/\mathrm{dln}(\overline{N_d})$) infers a $\overline{\mathrm{LWP}}$ response to $\overline{N_d}$ perturbation (Gryspeerdt et al., 2019). Here we estimate L_0 by performing linear regression on median values of $\overline{\mathrm{LWP}}$ in quartile bins of $\overline{N_d}$. MCCs present an overall negative $\overline{\mathrm{LWP}}$ response to $\overline{N_d}$ perturbation at all cell sizes (Figure 3a) with an average L_0 of −0.25. L_0 is more negative for non-precipitation dominant cells (quartile bins of $\overline{N_d}$ to the right of the dotted line in Figure 3a), indicating strong evidence of entrainment-related evaporation at cloud top that is strengthened with the increase of N_d, as a result of smaller cloud droplets and hence greater droplet surface area, as well as weaker cloud droplet sedimentation (evaporation-entrainment feedbacks, Ackerman et al., 2004; Bretherton et al., 2007; Wang et al., 2003). The negative LWP response for non-precipitating clouds is consistent with previous numerical and observational studies (e.g., Christensen & Stephens, 2011; Glassmeier et al., 2021; Gryspeerdt et al., 2019; Possner et al., 2020). For precipitation dominant cells (quartile bins of $\overline{N_d}$ to the left of the dotted line in Figure 3a), L_0 is less negative. This might be ascribed to precipitation-induced stabilization that weakens the entrainment drying effect. The fact that L_0 is less negative for precipitation dominant cells than for their non-precipitating counterparts leads us to conclude that the scavenging of cloud droplets due to precipitation from clouds with higher LWP (i.e., negative L_0) is marginal.

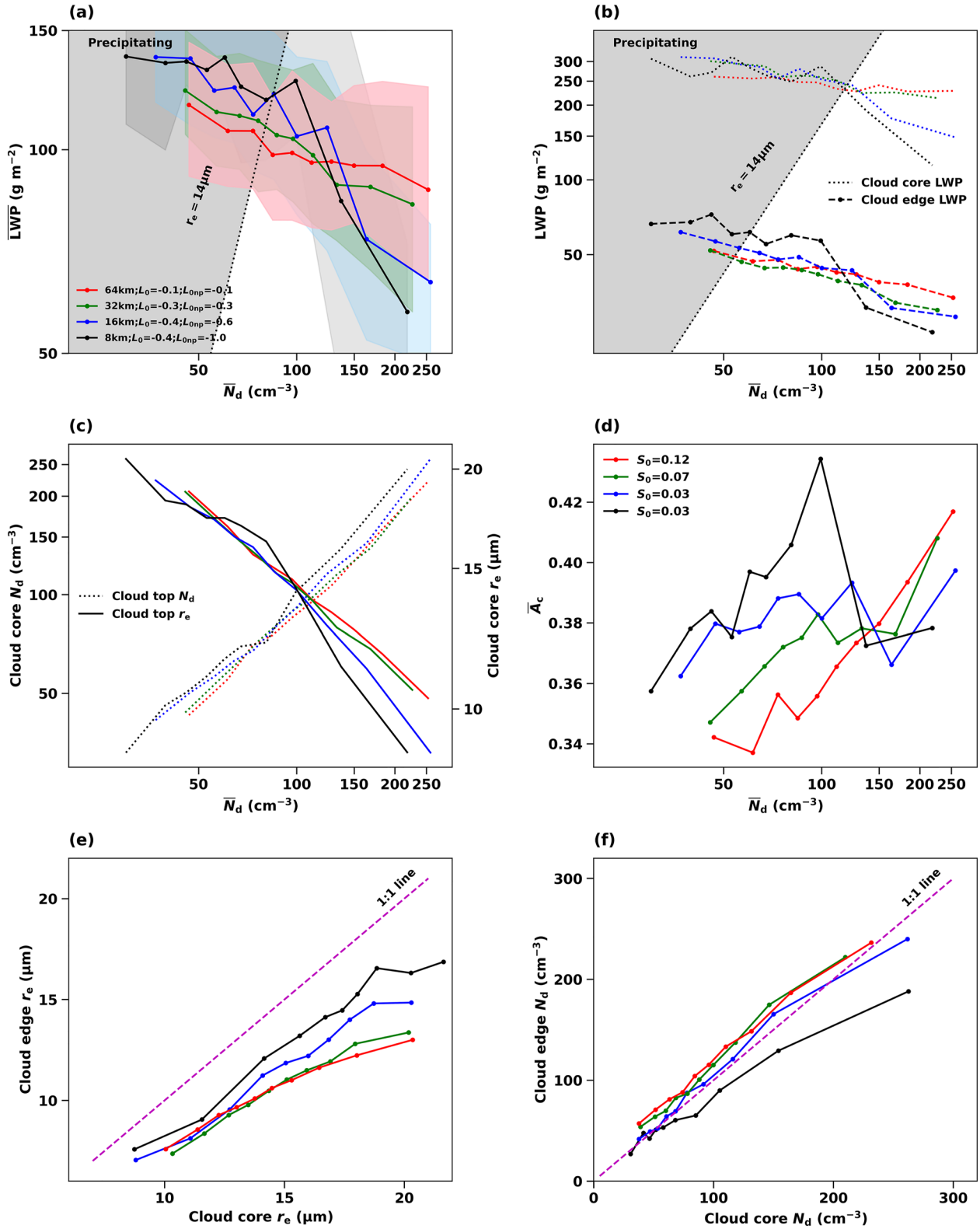

Figure 3. (a) Median and interquartile range of scene-average liquid water path (LWP) of cloudy pixels; (b) Median LWP at cloud cores and edges; (c) Median scene-average cloud core N_d and r_e; (d) median cloud albedo, in 10% percentile bins of scene-average N_d of cloudy pixels. Values are shown on logarithmic scales. (e) Median r_e at cloud edges in 10% percentile bins of r_e at cloud cores. (f) Same as (e) but for N_d. All panels are plotted for MCCs of 8 km (black), 16 km (blue), 32 km (green), and 64 km (red). The black dashed lines in (a and b) correspond to an adiabatic volume-mean droplet radius at cloud top of 14 μm (adiabatic condensation rate of 2.14×10^6 kg m^{-4}) following Glassmeier et al. (2019). Shades of gray background colors in (a and b) represent a general indicator of likelihood of precipitation.

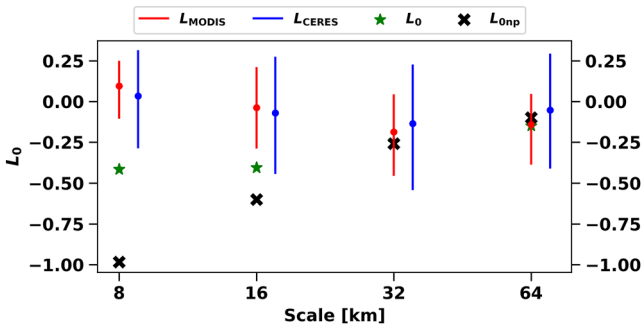

Figure 4. Aerosol-induced liquid water path (LWP) perturbation computed from scene-average LWP and N_d of the cloudy MODerate-resolution Imaging Spectroradiometer (MODIS) pixels as described in Section 4, for entire cloud deck ($L_0 = dln(\overline{LWP})/dln(\bar{N}_d)$, green stars) and for non-precipitation dominant MCCs (L_{0np}, black crosses). Red and blue lines indicate interquartile ranges of LWP adjustment computed on MODIS (~1 km; L_{MODIS}) and CERES (~0.2°; L_{CERES}) footprints respectively via the slope of linear regression within satellite snapshots of 2° × 2°. Dots represent the median values. Results are presented for MCCs of 8, 16, 32, and 64 km.

MCC L_0 depends notably on MCC cell size, especially for non-precipitation dominant cells (L_{0np}), where L_{0np} is significantly less negative for MCCs at larger cell sizes. L_{0np} is −0.1 for non-precipitation dominant MCCs at 64 km, and −1 at 8 km. The disparity in L_{0np} across cell sizes is reflected in both cloud cores and edges (Figure 3b), defined as the top 10% LWP and bottom 10%–20% LWP respectively in each scene (e.g., Figure 1). This implies that the L_{0np} difference is primarily caused by different efficiencies of entrainment-related evaporation that occurs both in cell cores and at cell edges, rather than changes in local precipitation that usually only occurs in cell cores. Moreover, the robust L_{0np} dependence on cell size, regardless of whether the analysis is for the entire cloud deck (Figure 3a), or for cloud cores, or cloud edges (Figure 3b), suggests that entrainment depletion of cloud water is ubiquitous throughout clouds, rather than being confined to cloud edges, where (i.e., cloud edges) free tropospheric air is usually mixed vertically throughout the boundary layer (Zhou & Bretherton, 2019b). This is consistent with Yamaguchi and Randall (2012) who find sizable entrainment in narrow cloud holes embedded in thick cloud cores where updrafts are dominant. The mixing of air from the free troposphere into the boundary layer within cloud cores can sometimes be intense enough to penetrate the clouds, leading to a comparable magnitude of turbulence below cloud cores and edges (Zhou & Bretherton, 2019a).

The weaker LWP response for large-scale MCCs implies less efficient entrainment-related evaporation (Figure 3a). Dynamically, this is supported by their weaker turbulence kinetic energy and lower entrainment rate at cloud top that diminishes the depletion of cloud water given the same aerosol concentration (e.g., Bretherton et al., 2007). Meanwhile, given the same surrounding aerosol concentration (represented by $\overline{N_d}$), the smaller number of larger cloud droplets in cloud cores further hampers the entrainment-related evaporation for large-scale MCCs in cloud cores (Figure 3c). At cloud edges, the number and size of cloud droplets are similar at a given $\overline{N_d}$ across scales (Figure S7), indicating that the disparity in L_0 at cloud edges (Figure 3b) is essentially dynamically driven. A comparison between cloud core and cloud edge r_e (Figure 3e) shows that cloud core droplets are larger than at cloud edges across all scales, especially for large-scale cells with large cloud core r_e (due to more positively skewed LWP distribution, as explained in Section 3). For large-scale cells, the number of droplets in cloud cores is generally smaller than at cloud edges, regardless of cloud core N_d (Figure 3f). The sensitivity of retrieved N_d to inhomogeneous adiabatic fraction is presented in Figure S8 of Supporting Information S1. We find the same qualitative dependence of N_d on cloud scale.

Small-scale MCCs present a neutral $\overline{A_c}$ response to $\overline{N_d}$ perturbations (as quantified by $S_0 = \mathrm{dln}(\overline{A_c})/\mathrm{dln}(\overline{N_d})$; Figure 3d), but an increasingly more positive response with increasing scale as a result of the weakening of the negative L_0 with increasing scale (Figure 3a). The noisy relationships at the smaller scales are likely due to the CERES footprint resolution (~0.2°) being coarser than the cloud scale. S_0 is 0.12 at 64 km and ~0.02–0.03 at 8 and 16 km. These numbers should be taken with caution because of the noisy S_0 slopes at small scales. Apart from S_0, the overall radiative effect of MCCs over a given ocean area also depends on cloud fraction. In Figure S9 of Supporting Information S1, we show an overall positive response of cloud fraction to $\overline{N_d}$ for MCCs at all scales, which tends to augment the radiative response of MCC to $\overline{N_d}$ associated with the cloud albedo response. Interestingly, the L_0 and S_0 differences across cell scales are found to be independent of seasonal variability and meteorological conditions (see more discussion in Figures S10 and S11 of Supporting Information S1).

5. Evaluation of Cloud Water Adjustment Computed on MODIS and CERES Footprints

In Figure 4, we quantify the cloud water adjustment computed on both MODIS (~1 km) and CERES (~0.2°) footprints, via the slope of linear regression between retrieved LWP and N_d within satellite snapshots of 2° × 2°, (hereafter L_{CERES} and L_{MODIS}). The results are classified by the four cloud scales derived from the wavelet analysis.

In contrast to the L_0 and L_{0np} shown in Section 4 that tend to become less negative with cloud scale, L_{MODIS} shows a clear decreasing trend with cloud scale—a bias originating from the intra-cell correlation between LWP and

N_d discussed in Section 3. The strongest bias is ∼120% for MCCs of 8 km where L_0 is the most negative while L_{MODIS} is the most positive. The discrepancy between L_0 and L_{MODIS} is unlikely to be caused by the potential bias in L_0 related to spatial aggregation, since the spatial averaging bias is shown to be often positive (Feingold et al., 2022). The bias in L_{MODIS} decreases with cloud scale. The good agreement between L_0 and L_{MODIS} for large scales is likely a coincidence (Figure 4).

With a coarser CERES footprint resolution (0.2°) that reduces the intra-cell impact to a certain extent, L_{CERES} lowers the positive bias in L_{MODIS} by ∼25% and ∼10% for MCCs of size 8 and 16 km respectively, yet L_{CERES} is much noisier and shows a similar decreasing trend with cloud scale. This suggests that L_{CERES} might still carry some remnant intra-cell bias. Additionally, the linear regression approach within satellite snapshots assumes implicitly that cloud response occurs over a relatively short time (if one relates longer times to larger spatial scales), which potentially excludes cases of strong negative cloud response that takes much longer to develop, either through the ∼1 day timescale for LWP adjustment (Glassmeier et al., 2021) or through slow boundary layer evolution (Bretherton et al., 2010). This likely contributes to the positive bias of L_{CERES}, especially for small scale MCCs where cloud top entrainment is strong.

6. Conclusions

This study presents an observed climatology of cloud water adjustment to aerosol-induced perturbations for closed MCC across different sizes (8, 16, 32, and 64 km) over the North Atlantic Ocean, using 7 years of MODIS cloud property retrievals. Our study suggests that MCC cell size plays a nontrivial role in regulating aerosol-induced brightness via cloud water adjustment: the inefficient depletion of cloud water with increasing cloud droplet number concentration (N_d) for large scale MCCs leads to a significant increase in cloud albedo for an increase in N_d compared to that for small scale MCCs (Figure 3d). This needs to be taken into consideration for improving projections of future MCC and climate change.

We find noticeable intra-cell co-variability between LWP, effective radius (r_e), and N_d that varies with cell size (Figure 2). For MCCs of relatively large size, fewer cloud droplets are found in thicker cell cores where the cloud droplets are much larger in size compared to cloud edges (Figures 3e and 3f). The LWP adjustment computed on MODIS footprints can lead to a positive bias as large as ∼120% due to intra-cell co-variability of LWP and N_d. Even the CERES footprint resolution is high enough to potentially carry some intra-cell bias. Lastly, one needs to be cautious when using N_d as a proxy for the surrounding aerosol. Averaging is recommended to avoid bias caused by N_d heterogeneity associated with small-scale, spatially varying updrafts within cloud cells. While strongly suggestive, the empirical analysis of the observational record in this study does not prove causality. For example, the retrieval errors of τ and r_e could potentially introduce a significant bias in L_0 (Arola et al., 2022). Future studies are encouraged in this regard.

Data Availability Statement

We acknowledge the cloud properties from the MODIS on the Aqua satellite: https://ladsweb.modaps.eosdis.nasa.gov/archive/allData/61/MYD06_L2/; the Clouds and Earth's Radiant Energy System (CERES)'s Single Scanner Footprint level 2 Edition 4A data set at https://ceres-tool.larc.nasa.gov/ord-tool/products?CERESProducts=SS-Flevel2_Ed4; the ECMWF's fifth generation atmospheric reanalysis (ERA5) data at https://doi.org/10.24381/cds.bd0915c6. The processed MCC data is stored in the following NOAA data archive: https://csl.noaa.gov/groups/csl9/datasets/data/cloud_phys/2023-Zhou/.

Acknowledgments
We gratefully acknowledge funding from the U.S. Department of Energy, Office of Science, Atmospheric System Research Program Interagency Award 89243020SSC000055 and from an Earth's Radiation Budget Grant, NOAA CPO Climate CI 03-01-07-001.

References

Ackerman, A. S., Kirkpatrick, M. P., Stevens, D. E., & Toon, O. B. (2004). The impact of humidity above stratiform clouds on indirect aerosol climate forcing. *Nature*, *432*(7020), 1014–1017. https://doi.org/10.1038/nature03174

Agee, E. M., Chen, T. S., & Dowell, K. E. (1973). A review of mesoscale cellular convection. *Bulletin of the American Meteorological Society*, *54*(10), 1004–1012. https://doi.org/10.1175/1520-0477(1973)054<1004:aromcc>2.0.co;2

Albrecht, B. A. (1989). Aerosols, cloud microphysics, and fractional cloudiness. *Science*, *245*(4923), 1227–1230. https://doi.org/10.1126/science.245.4923.1227

Albrecht, B. A., Fairall, C. W., Thomson, D. W., White, A. B., Snider, J. B., & Schubert, W. H. (1990). Surface-based remote sensing of the observed and the adiabatic liquid water content of stratocumulus clouds. *Geophysical Research Letters*, *17*(1), 89–92. https://doi.org/10.1029/gl017i001p00089

Arola, A., Lipponen, A., Kolmonen, P., Virtanen, T. H., Bellouin, N., Grosvenor, D. P., et al. (2022). Aerosol effects on clouds are concealed by natural cloud heterogeneity and satellite retrieval errors. *Nature Communications*, *13*(1), 7357. https://doi.org/10.1038/s41467-022-34948-5

Bretherton, C. S., Blossey, P. N., & Uchida, J. (2007). Cloud droplet sedimentation, entrainment efficiency, and subtropical stratocumulus albedo. *Geophysical Research Letters*, *34*(3), L03813. https://doi.org/10.1029/2006gl027648

Bretherton, C. S., Uchida, J., & Blossey, P. N. (2010). Slow manifolds and multiple equilibria in stratocumulus-capped boundary layers. *Journal of Advances in Modeling Earth Systems*, *2*(4). https://doi.org/10.3894/james.2010.2.14

Cahalan, R. F., Ridgway, W., Wiscombe, W. J., Bell, T. L., & Snider, J. B. (1994). The albedo of fractal stratocumulus clouds. *Journal of the Atmospheric Sciences*, *51*(16), 2434–2455. https://doi.org/10.1175/1520-0469(1994)051<2434:taofsc>2.0.co;2

Chen, Y. C., Christensen, M. W., Stephens, G. L., & Seinfeld, J. H. (2014). Satellite-based estimate of global aerosol–cloud radiative forcing by marine warm clouds. *Nature Geoscience*, *7*(9), 643–646. https://doi.org/10.1038/ngeo2214

Christensen, M. W., & Stephens, G. L. (2011). Aerosol and Clouds-D03201 Microphysical and macrophysical responses of marine stratocumulus polluted by underlying ships: Evidence of cloud deepening. *Journal of Geophysical Research-Part D-Atmospheres*, *116*(3), D03201. https://doi.org/10.1029/2010jd014638

Danker, J., Sourdeval, O., McCoy, I. L., Wood, R., & Possner, A. (2021). Exploring relations between cloud morphology, cloud phase, and cloud radiative properties in Southern ocean stratocumulus clouds. *Atmospheric Chemistry and Physics Discussions*, 1–26.

Daubechies, I. (1988). Orthonormal bases of compactly supported wavelets. *Communications on Pure and Applied Mathematics*, *41*(7), 909–996. https://doi.org/10.1002/cpa.3160410705

Daubechies, I., & Bates, B. J. (1993). Ten lectures on wavelets.

Eastman, R., McCoy, I. L., & Wood, R. (2021). Environmental and internal controls on Lagrangian transitions from closed cell mesoscale cellular convection over subtropical oceans. *Journal of the Atmospheric Sciences*, *78*(8), 2367–2383. https://doi.org/10.1175/jas-d-20-0277.1

Feingold, G., Goren, T., & Yamaguchi, T. (2022). Quantifying albedo susceptibility biases in shallow clouds. *Atmospheric Chemistry and Physics*, *22*(5), 3303–3319. https://doi.org/10.5194/acp-22-3303-2022

Geerts, B., Giangrande, S. E., McFarquhar, G. M., Xue, L., Abel, S. J., Comstock, J. M., et al. (2022). The COMBLE campaign: A study of marine boundary-layer clouds in Arctic cold-air outbreaks. *Bulletin of the American Meteorological Society*, *103*(5), E1371–E1389. https://doi.org/10.1175/bams-d-21-0044.1

Glassmeier, F., Hoffmann, F., Johnson, J. S., Yamaguchi, T., Carslaw, K. S., & Feingold, G. (2019). An emulator approach to stratocumulus susceptibility. *Atmospheric Chemistry and Physics*, *19*(15), 10191–10203. https://doi.org/10.5194/acp-19-10191-2019

Glassmeier, F., Hoffmann, F., Johnson, J. S., Yamaguchi, T., Carslaw, K. S., & Feingold, G. (2021). Aerosol-cloud-climate cooling overestimated by ship-track data. *Science*, *371*(6528), 485–489. https://doi.org/10.1126/science.abd3980

Grosvenor, D. P., Sourdeval, O., Zuidema, P., Ackerman, A., Alexandrov, M. D., Bennartz, R., et al. (2018). Remote sensing of droplet number concentration in warm clouds: A review of the current state of knowledge and perspectives. *Reviews of Geophysics*, *56*(2), 409–453. https://doi.org/10.1029/2017rg000593

Gryspeerdt, E., Goren, T., Sourdeval, O., Quaas, J., Mülmenstädt, J., Dipu, S., et al. (2019). Constraining the aerosol influence on cloud liquid water path. *Atmospheric Chemistry and Physics*, *19*(8), 5331–5347. https://doi.org/10.5194/acp-19-5331-2019

Jensen, M. P., Ghate, V. P., Wang, D., Apoznanski, D. K., Bartholomew, M. J., Giangrande, S. E., et al. (2021). Contrasting characteristics of open-and closed-cellular stratocumulus cloud in the eastern North Atlantic. *Atmospheric Chemistry and Physics*, *21*(19), 14557–14571. https://doi.org/10.5194/acp-21-14557-2021

Kazil, J., Yamaguchi, T., & Feingold, G. (2017). Mesoscale organization, entrainment, and the properties of a closed-cell stratocumulus cloud. *Journal of Advances in Modeling Earth Systems*, *9*(5), 2214–2229. https://doi.org/10.1002/2017ms001072

Lang, F., Ackermann, L., Huang, Y., Truong, S. C., Siems, S. T., & Manton, M. J. (2022). A climatology of open and closed mesoscale cellular convection over the Southern Ocean derived from Himawari-8 observations. *Atmospheric Chemistry and Physics*, *22*(3), 2135–2152. https://doi.org/10.5194/acp-22-2135-2022

Mallat, S. G. (1989a). Multifrequency channel decompositions of images and wavelet models. *IEEE Transactions on Acoustics*, *37*(12), 2091–2110. https://doi.org/10.1109/29.45554

Mallat, S. G. (1989b). A theory for multiresolution signal decomposition: The wavelet representation. *IEEE Transactions on Pattern Analysis and Machine Intelligence*, *11*(7), 674–693. https://doi.org/10.1109/34.192463

McCoy, I. L., McCoy, D. T., Wood, R., Zuidema, P., & Bender, F. A.-M. (2022). The role of mesoscale cloud morphology in the shortwave cloud feedback. https://doi.org/10.1002/essoar.10512288.1

McCoy, I. L., Wood, R., & Fletcher, J. K. (2017). Identifying meteorological controls on open and closed mesoscale cellular convection associated with marine cold air outbreaks. *Journal of Geophysical Research: Atmospheres*, *122*(21), 11–678. https://doi.org/10.1002/2017jd027031

Meyer, Y. (1992). *Wavelets and operators: Volume 1* (Vol. 37). Cambridge University Press.

Minnis, P., Sun-Mack, S., Chen, Y., Chang, F. L., Yost, C. R., Smith, W. L., et al. (2020). CERES MODIS cloud product retrievals for edition 4—Part I: Algorithm changes. *IEEE Transactions on Geoscience and Remote Sensing*, *59*(4), 2744–2780. https://doi.org/10.1109/tgrs.2020.3008866

Nakajima, T., & King, M. D. (1990). Determination of the optical thickness and effective particle radius of clouds from reflected solar radiation measurements. Part I: Theory. *Journal of the Atmospheric Sciences*, *47*(15), 1878–1893. https://doi.org/10.1175/1520-0469(1990)047<1878:dotota>2.0.co;2

Nicholls, S. (1987). A model of drizzle growth in warm, turbulent, stratiform clouds. *Quarterly Journal of the Royal Meteorological*.

Platnick, S., Ackerman, S., King, M., Meyer, K., Menzel, W. P., Holz, R. E., et al. (2015). *MODIS atmosphere L2 cloud product (06_L2). NASA MODIS adaptive processing system*. Goddard Space Flight Center. https://doi.org/10.5067/MODIS/MOD06_L2.006

Platnick, S., King, M. D., Ackerman, S. A., Menzel, W. P., Baum, B. A., Riédi, J. C., & Frey, R. A. (2003). The MODIS cloud products: Algorithms and examples from Terra. *IEEE Transactions on Geoscience and Remote Sensing*, *41*(2), 459–473. https://doi.org/10.1109/tgrs.2002.808301

Possner, A., Eastman, R., Bender, F., & Glassmeier, F. (2020). Deconvolution of boundary layer depth and aerosol constraints on cloud water path in subtropical stratocumulus decks. *Atmospheric Chemistry and Physics*, *20*(6), 3609–3621. https://doi.org/10.5194/acp-20-3609-2020

Stephens, G. L. (1986). Radiative transfer in spatially heterogeneous, two-dimensional, anisotropically scattering media. *Journal of Quantitative Spectroscopy and Radiative Transfer*, *36*(1), 51–67. https://doi.org/10.1016/0022-4073(86)90015-4

Terai, C. R., Bretherton, C. S., Wood, R., & Painter, G. (2014). Aircraft observations of aerosol, cloud, precipitation, and boundary layer properties in pockets of open cells over the southeast Pacific. *Atmospheric Chemistry and Physics*, *14*(15), 8071–8088. https://doi.org/10.5194/acp-14-8071-2014

Tornow, F., Ackerman, A. S., & Fridlind, A. M. (2021). Preconditioning of overcast-to-broken cloud transitions by riming in marine cold air outbreaks. *Atmospheric Chemistry and Physics*, *21*(15), 12049–12067. https://doi.org/10.5194/acp-21-12049-2021

Wang, S., Wang, Q., & Feingold, G. (2003). Turbulence, condensation, and liquid water transport in numerically simulated nonprecipitating stratocumulus clouds. *Journal of the Atmospheric Sciences*, *60*(2), 262–278. https://doi.org/10.1175/1520-0469(2003)060<0262:tcalwt>2.0.co;2

Wood, R., & Bretherton, C. S. (2006). On the relationship between stratiform low cloud cover and lower-tropospheric stability. *Journal of Climate*, *19*(24), 6425–6432. https://doi.org/10.1175/jcli3988.1

Wood, R., & Taylor, J. P. (2001). Liquid water path variability in unbroken marine stratocumulus cloud. *Quarterly Journal of the Royal Meteorological Society*, *127*(578), 2635–2662. https://doi.org/10.1002/qj.49712757807

Yamaguchi, T., & Randall, D. A. (2012). Cooling of entrained parcels in a large-eddy simulation. *Journal of the Atmospheric Sciences*, *69*(3), 1118–1136. https://doi.org/10.1175/jas-d-11-080.1

Yuan, T., Song, H., Wood, R., Mohrmann, J., Meyer, K., Oreopoulos, L., & Platnick, S. (2020). Applying deep learning to NASA MODIS data to create a community record of marine low-cloud mesoscale morphology. *Atmospheric Measurement Techniques*, *13*(12), 6989–6997. https://doi.org/10.5194/amt-13-6989-2020

Zhang, J., Zhou, X., Goren, T., & Feingold, G. (2022). Albedo susceptibility of northeastern Pacific stratocumulus: The role of covarying meteorological conditions. *Atmospheric Chemistry and Physics*, *22*(2), 861–880. https://doi.org/10.5194/acp-22-861-2022

Zhou, X., Ackerman, A. S., Fridlind, A. M., & Kollias, P. (2018). Simulation of mesoscale cellular convection in marine stratocumulus. Part I: Drizzling conditions. *Journal of the Atmospheric Sciences*, *75*(1), 257–274. https://doi.org/10.1175/jas-d-17-0070.1

Zhou, X., & Bretherton, C. S. (2019a). The correlation of mesoscale humidity anomalies with mesoscale organization of marine stratocumulus from observations over the ARM Eastern North Atlantic site. *Journal of Geophysical Research: Atmospheres*, *124*(24), 14059–14071. https://doi.org/10.1029/2019jd031056

Zhou, X., & Bretherton, C. S. (2019b). Simulation of mesoscale cellular convection in marine stratocumulus: 2. Nondrizzling conditions. *Journal of Advances in Modeling Earth Systems*, *11*(1), 3–18. https://doi.org/10.1029/2018ms001448

Zhou, X., Bretherton, C. S., Eastman, R., McCoy, I. L., & Wood, R. (2021). Wavelet analysis of properties of marine boundary layer mesoscale cells observed from AMSR-E. *Journal of Geophysical Research: Atmospheres*, *126*(14), e2021JD034666. https://doi.org/10.1029/2021jd034666

Zhou, X., Heus, T., & Kollias, P. (2017). Influences of drizzle on stratocumulus cloudiness and organization. *Journal of Geophysical Research: Atmospheres*, *122*(13), 6989–7003. https://doi.org/10.1002/2017jd026641

Zhou, X., Zhang, J., & Feingold, G. (2021). On the importance of sea surface temperature for aerosol-induced brightening of marine clouds and implications for cloud feedback in a future warmer climate. *Geophysical Research Letters*, *48*(24), e2021GL095896. https://doi.org/10.1029/2021gl095896